

Magnetotransport in overdoped $\text{La}_{2-x}\text{Sr}_x\text{CuO}_4$: Fermi liquid approachRui-Ying Mao,¹ Da Wang^{1,2,*}, Congjun Wu,^{3,4,†} and Qiang-Hua Wang^{1,2,‡}¹National Laboratory of Solid State Microstructures and School of Physics, Nanjing University, Nanjing 210093, China²Collaborative Innovation Center of Advanced Microstructures, Nanjing University, Nanjing 210093, China³School of Science, Westlake University, Hangzhou, Zhejiang 310024, China⁴Key Laboratory for Quantum Materials of Zhejiang Province, School of Science, Westlake University, 18 Shilongshan Road, Hangzhou 310024, Zhejiang Province, China

(Received 11 January 2021; revised 18 June 2021; accepted 24 June 2021; published 6 July 2021)

Recently, several experiments on $\text{La}_{2-x}\text{Sr}_x\text{CuO}_4$ (LSCO) challenged the Fermi liquid picture for overdoped cuprates and stimulated intensive debates. In this work, we study the magnetotransport phenomena in such systems based on the Fermi liquid assumption. The Hall coefficient R_H and magnetoresistivity ρ_{xx} are investigated near the Van Hove singularity (VHS) $x_{\text{VHS}} \approx 0.2$ across which the Fermi surface topology changes from hole- to electronlike. The main results are (1) R_H drops from positive to negative values with increasing B in the doping regime $x_{\text{VHS}} < x \lesssim 0.3$ and (2) ρ_{xx} grows as B^2 at small B and saturates at large B , while a “nearly linear” dependence shows up in the transition regime, which is significantly enlarged near the VHS. These results can be tested by future magnetotransport experiments in overdoped LSCO to check whether the Fermi liquid picture applies or not.

DOI: [10.1103/PhysRevB.104.024501](https://doi.org/10.1103/PhysRevB.104.024501)**I. INTRODUCTION**

After more than three decades of efforts, there still exist many mysteries in cuprate superconductors, partly because the superconductivity arises from two fundamentally different states: the parent undoped Mott insulating state and the heavily overdoped metallic state [1]. Close to the Mott insulator side, only doped holes contribute to charge transport, and the carrier density equals the doping level x (per Cu). On the other hand, in the heavily overdoped metallic region, the total carrier density is expected to change to $1 + x$. Such an anticipated transition from x to $1 + x$ was reported to occur at a critical doping level x^* by measuring the normal state Hall number n_H in $\text{YBa}_2\text{Cu}_3\text{O}_y$ (YBCO) [2] and $\text{La}_{1.6-x}\text{Nd}_{0.4}\text{Sr}_x\text{CuO}_4$ (Nd-LSCO) [3] under strong magnetic field. Here, n_H is defined as $\frac{V}{eR_H}$, with R_H being the Hall coefficient and V being the volume per Cu, such that the sign of n_H indicates the carrier type. In combination with many other experiments [4–6], the sharp transition of n_H from x to $1 + x$ is possibly driven by an underlying quantum critical point (QCP) beneath the superconducting dome [7–14].

However, as for the case of Nd-LSCO, there exists a puzzle: at $x > x_{\text{VHS}} \approx 0.22$, where x_{VHS} is the doping when the Fermi energy reaches the Van Hove singularity (VHS) [15,16], $n_H = 1 + x$ is in conflict with the prediction of the Lifshitz-Azbel-Kagonov theory [17,18]. It states that in the strong magnetic field limit, the Hall number n_H should be given by the electron number enclosed by the Fermi surface (FS), i.e., $n_H = -(1 - x)$, where the minus sign indicates the carriers are electrons rather than holes. On the other

hand, if the magnetic field value B is not large enough, the Hall number is not determined by the Luttinger volume [19] directly but depends on the FS curvature [20]; hence, $n_H = 1 + x$ is not anticipated directly either. Therefore, how to explain $n_H = 1 + x$ at $x > x_{\text{VHS}}$ remains an open question. One possibility may be the failure of the Fermi liquid description.

Different from YBCO and Nd-LSCO, the transition from x to $1 + x$ has not been observed in $\text{La}_{2-x}\text{Sr}_x\text{CuO}_4$ (LSCO). Like for Nd-LSCO, there also exists a VHS at $x_{\text{VHS}} \approx 0.18\text{--}0.20$, as observed by the angle-resolved photoemission spectroscopy (ARPES) experiment [21]. One consequence of the VHS is that the normal state Hall coefficient R_H decreases smoothly with doping and finally drops to negative values at $x \approx 0.3$ in the weak magnetic field limit [22–24]. In fact, the smooth behavior of R_H upon doping is consistent with the measurements of the upper critical field [25], superfluid density [26], and resistivity [27] in LSCO. Certainly, some experiments reported possible QCP signatures such as the insulator-to-metal transition around the optimal doping $x_c \approx 0.16$ [28] and the vanishing of the stripe/nematic order [29–31], accompanied by a peak [32] or upturn in n_H [33] upon doping at low temperatures under strong magnetic fields. Further evidence of the QCP comes from the observation of the linear magnetoresistivity at $0.16 < x < 0.19$ which was attributed phenomenologically to the linear scattering rate $\tau^{-1} \propto B$ [34], which is similar to the Planckian dissipation [35]. However, such an explanation is based on the assumption that the B dependence comes from only τ^{-1} , which still needs more careful exploration. Nevertheless, these experiments, together with the observation of nematicity [30] and the very low superfluid density [26], have stimulated debate on whether the metallic states in overdoped cuprates are Fermi liquids or not [36].

*dawang@nju.edu.cn

†wucongjun@westlake.edu.cn

‡qhwang@nju.edu.cn

Motivated by this experimental progress, we performed the present study in order to check whether the overdoped LSCO is within the Fermi liquid picture or not. We employ Chambers's semiclassical theory [37,38] to study the Hall coefficient and magnetoresistivity for the general values of the magnetic field B . This study is based on the semiclassical cyclotron orbits of quasiparticles on the Fermi surface. It should be pointed out that the frequently used result of $R_H = \frac{1}{qn}$ is incorrect except for parabolic dispersions (with a circular FS) or in the strong-field limit [17,18]; otherwise, it should be determined by the FS curvature in the weak-field regime, as pointed out by Ong [20]. Based on Chambers's formula, our calculations show the Hall coefficient changes sign with increasing field strengths in the range of doping $x_{\text{VHS}} < x \lesssim 0.3$. Furthermore, there exists a "nearly linear" magnetoresistivity at intermediate field strengths, especially when doping is close to the VHS, thus providing an alternative explanation for the B -linear resistivity other than assuming $\tau^{-1} \propto B$. These results are consistent with the known experiments, indicating that the magnetotransport properties of the overdoped LSCO may still be described by the Fermi liquid theory.

II. MODEL AND METHOD

To capture the band structure of the overdoped LSCO, we adopt the single-band model on the square lattice,

$$H = - \sum_{(ij)\sigma} (t_{ij} c_{i\sigma}^\dagger c_{j\sigma} + \text{H.c.}) - \mu \sum_{i\sigma} c_{i\sigma}^\dagger c_{i\sigma}, \quad (1)$$

where t_{ij} is the hopping between sites i and j and μ is the chemical potential. To be specific, we denote t , $t' = -0.12t$ and $t'' = 0.06t$ as the first-, second-, and third-nearest-neighbor hoppings obtained by fitting the ARPES experiments [39]. With these parameters, the band dispersion is given by $\varepsilon_{\mathbf{k}} = -2t \cos(k_x) - 2t \cos(k_y) - 4t' \cos(k_x) \cos(k_y) - 2t'' \cos(2k_x) - 2t'' \cos(2k_y) - \mu$. When μ matches the VHS, $\mu_{\text{VHS}} = 4t' - 4t''$, corresponding to the doping $x_{\text{VHS}} \approx 0.197$. Three typical Fermi surfaces near the VHS are plotted in Fig. 1. At $x < x_{\text{VHS}}$, the FS is holelike surrounding (π, π) , i.e., the corner of the Brillouin zone (BZ). At $x > x_{\text{VHS}}$, the FS changes to surround the center of the BZ, which is globally electronlike. Nevertheless, the local curvatures of the FS segments change signs from electronlike in the antinodal region [close to $(\pi, 0)$ and $(0, \pi)$] to holelike in the nodal region [close to $(\pm\frac{\pi}{2}, \pm\frac{\pi}{2})$], leading to a multicomponent feature [20]. Which picture (global or local) is more relevant for the Hall experiments is an interesting question.

The key lies in the ratio of the scattering lifetime τ relative to the cyclotron period \mathcal{T} . The cyclotron frequency $\omega_c = \frac{2\pi}{\mathcal{T}}$ is determined by the cyclotron mass $m_c = \frac{1}{2\pi} \frac{\partial S}{\partial \varepsilon}$ (S is the area surrounded by the cyclotron orbit with energy ε) through the relation $\omega_c = \frac{eB}{m_c}$. If τ is much larger than \mathcal{T} , i.e., $\omega_c \tau \gg 1$, the cyclotron motion completes the entire orbit, leading to the global picture of the electronlike FS. Consequently, the Hall number n_H is anticipated to be the electron number surrounded by the FS [17] according to the Luttinger theorem [19], i.e., $n_H = 1 + x$ for $x < x_{\text{VHS}}$ and $n_H = -(1 - x)$

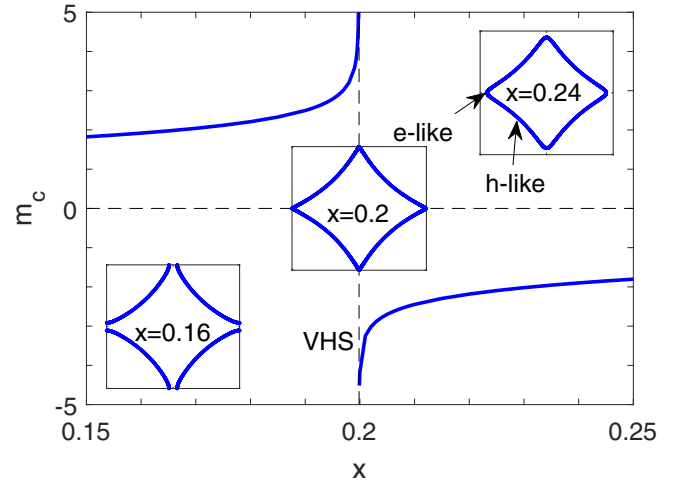


FIG. 1. Cyclotron mass m_c (in units of $\frac{\hbar^2}{a^2t}$) vs x . The VHS is shown by the vertical dashed line. The three insets show the FS below ($x = 0.16$), almost at ($x = 0.20$), and above ($x = 0.24$) the VHS filling. Two arrows indicate hole- and electronlike FS segments in the case of $x = 0.24$.

for $x > x_{\text{VHS}}$. Meanwhile, the resistivity should be roughly proportional to the cyclotron mass $|m_c|$. In contrast, if $\omega_c \tau \ll 1$, the quasiparticles have no chance to "see" the whole FS without scattering, and thus, the local picture is preferred. As a result, we cannot identify n_H as the carrier density directly, and the resistivity should be determined by the band mass $m_{\alpha\beta}^{-1} = \frac{\partial^2 \varepsilon}{\partial k_\alpha \partial k_\beta}$ rather than the cyclotron mass $|m_c|$.

In order to obtain a unified description connecting the above two limits, we adopt the semiclassical Chambers's formula [18,37,38],

$$\sigma_{\alpha\beta} = \frac{e^3 B}{(2\pi)^2} \int d\varepsilon \left(-\frac{\partial f_0}{\partial \varepsilon} \right) \times \int_0^{\mathcal{T}} dt v_\alpha(t) \int_{-\infty}^t dt' v_\beta(t') e^{-(t-t')/\tau}, \quad (2)$$

where $v_\alpha = \frac{\partial \varepsilon}{\partial k_\alpha}$ depends on t through the relation $\mathbf{k}(t)$. Eq. 2 is derived based on the Boltzmann's transport equation by considering the cyclotron motion perpendicular to \mathbf{B} . In cuprates, such a semiclassical picture can be justified by the observations of quantum oscillations [40] and cyclotron resonances [41], which mean quasiparticles remain coherent in magnetotransports. We focus on the situation with \mathbf{B} perpendicular to the ab -plane as in many experiment setups.

At low temperatures, only one cyclotron orbit, i.e., the FS, is needed to be considered. The electron motion is determined by the Lorentz force $\hbar \dot{\mathbf{k}} = -e \mathbf{v}_{\mathbf{k}} \times \mathbf{B}$. After the velocity $\mathbf{v}(t)$ is obtained (in this work by numerics), which satisfies the periodic condition $\mathbf{v}(t) = \mathbf{v}(t + \mathcal{T})$, it can be derived that [9]

$$\sigma_{\alpha\beta} = \frac{e^3 B}{(2\pi)^2} \frac{1}{1 - e^{-\mathcal{T}/\tau}} \times \int_0^{\mathcal{T}} dt v_\alpha(t) \int_{t-\mathcal{T}}^t dt' v_\beta(t') e^{-(t-t')/\tau}. \quad (3)$$

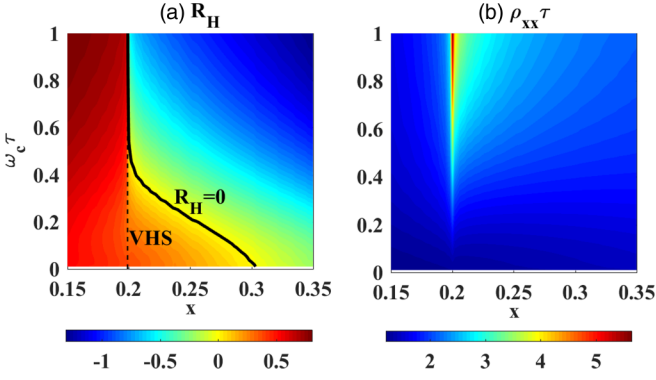


FIG. 2. Phase diagrams of (a) R_H and (b) $\rho_{xx}\tau$ as functions of x and $\omega_c\tau$. The color encodes the values of R_H (in units of $\frac{a^2c}{e}$) and $\rho_{xx}\tau$ (in units of $\frac{\hbar^2c}{e^2\tau}$). In (a), the contour of $R_H = 0$ is shown as the solid line which merges to the VHS (dashed line) at large $\omega_c\tau$.

Then the Hall coefficient R_H and magnetoresistivity ρ_{xx} follow directly,

$$R_H = \frac{\sigma_{xy}}{(\sigma_{xx}^2 + \sigma_{xy}^2)B}, \quad \rho_{xx} = \frac{\sigma_{xx}}{(\sigma_{xx}^2 + \sigma_{xy}^2)}. \quad (4)$$

Based on Eq. (5), $\frac{\sigma_{\alpha\beta}}{\tau}$ are functions of $\omega_c\tau$, yielding Kohler's relations [38,42]: $R_H = F(\omega_c\tau)$ and $\rho_{xx}\tau = G(\omega_c\tau)$, where F and G are functions of $\omega_c\tau$.

Both the weak- and strong-field limits have been extensively studied in the literature. When $\omega_c\tau \ll 1$, due to the exponential factor $e^{-(t-t')/\tau}$, the t' integral mainly comes from $t' \approx t$. Therefore, we can expand $v_\beta(t') = v_\beta(t) + \frac{\partial v_\beta}{\partial t}(t' - t)$ and substitute it into Eq. (2), giving

$$J_\alpha = e^2\tau \int_{\mathbf{k}} \left(-\frac{\partial f_0}{\partial \varepsilon_{\mathbf{k}}} \right) v_\alpha(\mathbf{k}) v_\beta(\mathbf{k}) E_\beta + e^3\tau^2 \int_{\mathbf{k}} \left(-\frac{\partial f_0}{\partial \varepsilon_{\mathbf{k}}} \right) v_\alpha(\mathbf{k}) \frac{\partial v_\beta(\mathbf{k})}{\partial k_\gamma} E_\beta (\mathbf{v}_{\mathbf{k}} \times \mathbf{B})_\gamma, \quad (5)$$

which is the same as the result obtained with Kubo's formula [43] and widely used in previous works [7,8,10,11]. On the other hand, in the strong-field limit, $\omega_c\tau \gg 1$, the exponential factor $e^{-(t-t')/\tau}$ can be approximated by unity, leading to $\sigma_{xy} = \frac{qn}{B}$, where $q = e$ ($-e$) when $m_c > 0$ (< 0) and n counts the electron number surrounded by the FS [17,18]. Then, $R_H = \frac{1}{qn}$ follows immediately due to the scaling behavior of $\sigma_{xx} \propto (\omega_c\tau)^{-2}$. Unfortunately, no simple results exist for ρ_{xx} in the strong-field limit in general [42].

III. RESULTS

Our main results are shown in Fig. 2. At first glance, both R_H and $\rho_{xx}\tau$ show significant dependence on $\omega_c\tau$, exhibiting different behaviors from free electrons in the Drude theory. In the strong-field limit $\omega_c\tau \rightarrow \infty$, R_H changes exactly at $x = x_{\text{VHS}}$, reflecting the topological change in the FS, and $\rho_{xx}\tau$ diverges similar to the behavior of an open orbit. On the other hand, in the weak-field limit, $\omega_c\tau \rightarrow 0$, both R_H and $\rho_{xx}\tau$ evolve smoothly with x . The mismatch between the above two limits leads to many interesting phenomena. In the following, let us undertake detailed discussions of R_H and ρ_{xx} .

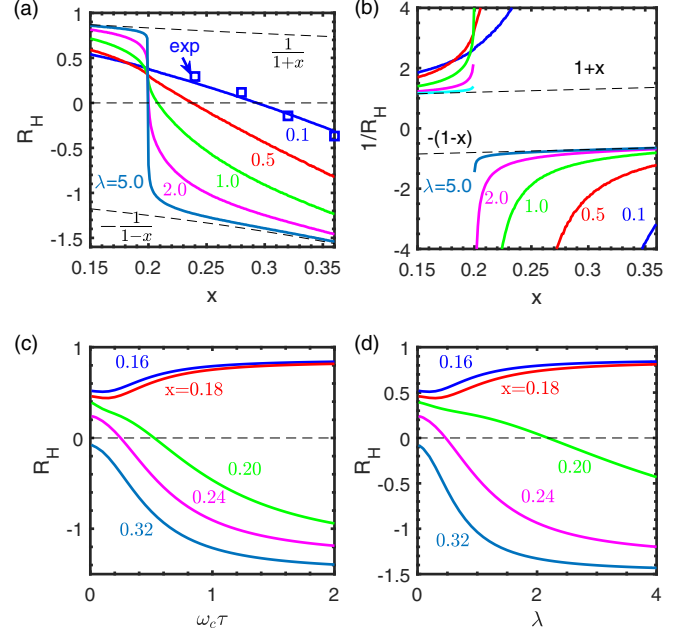


FIG. 3. (a) R_H and (b) $\frac{1}{R_H}$ are plotted vs the doping x . Each curve corresponds to a different value of $\lambda = \frac{eB\tau}{m^*}$. The experimental data for R_H at 300 K [24] in the weak-field limit are shown as squares. The strong-field limits $R_H = \pm \frac{1}{1 \pm x}$ are also plotted by the dashed lines for comparison. We plot R_H vs (c) $\omega_c\tau$ and (d) λ at fixed doping levels of x .

Before moving forward, let us combine the scattering lifetime τ and the magnetic field B into a dimensionless quantity $\lambda = \frac{eB\tau}{m^*}$, where $m^* = \frac{\hbar^2}{ta^2}$ is the band mass at the band bottom, with a being the lattice constant. λ is insensitive to doping, and it equals $\omega_c\tau$ at the band bottom. (In comparison, $\omega_c\tau$ strongly depends on x as the cyclotron mass m_c varies significantly with x near the VHS.) But close to the VHS, since $|m_c|$ is greatly enhanced, $\lambda \gg \omega_c\tau$. The values of λ are estimated below. We choose $t \approx 0.25$ eV as obtained from ARPES [21] and lattice constants $a \approx 3.8$ Å, $c \approx 6.6$ Å. The scattering rate τ^{-1} , however, is somewhat more difficult to determine. Upon doping, the interaction-induced scattering may become weaker, but the extrinsic disorder effect may become stronger. $\tau^{-1} \sim 5$ meV is roughly estimated from the optical conductivity measurements in overdoped LSCO [44], in agreement with the very recent measurement in optimally doped LSCO [41]. With these parameters, $\lambda \approx 0.01B$ (teslas). Therefore, the magnetic field used in the experiments $B \leq 80$ T [27,34] corresponds to $\lambda \leq 0.8$.

Typical behaviors of R_H are explicitly shown in Fig. 3. The most obvious feature is that its field dependence is very different from that of free electrons with parabolic dispersions. Figures 3(a) and 3(b) show that only in the strong-field limit, $\lambda \gg 1$ is R_H given by counting the carrier numbers, i.e., $eR_H = \frac{1}{1+x}$ and $-\frac{1}{1-x}$ when $x < x_{\text{VHS}}$ and $x > x_{\text{VHS}}$, respectively, although the discontinuity of R_H is smoothed by the finite lifetime. However, this relation breaks down for weaker fields. The experimental data for R_H in LSCO [22–24] are also plotted: R_H exhibits a significant deviation from the scaling of $-\frac{1}{1-x}$ and changes sign at $x \approx 0.3$. As shown in Fig. 3(c),

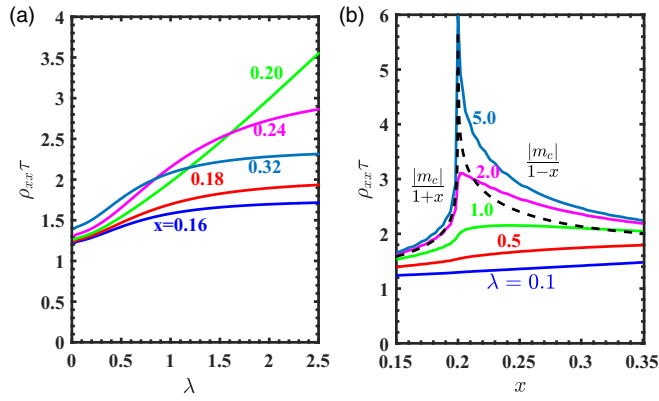


FIG. 4. (a) Field and (b) doping dependence of $\rho_{xx}\tau$. In (b), we also plot a rough estimation of $\rho_{xx}\tau \approx \frac{|m_c|}{1+x}$, which qualitatively describes the behavior in the strong-field limit.

R_H changes significantly with varying $\omega_c\tau$. The interesting regime lies in $x_{\text{VHS}} < x \lesssim 0.3$, where R_H drops from positive to negative values with increasing the field strength, and finally, it saturates to the strong-field limit $-\frac{1}{1-x}$. Near the VHS, although R_H changes sign at a finite value of $\omega_c\tau$, it requires a large field strength due to the divergence of m_c , which may be beyond the experimental availability. The field dependence of R_H is replotted in Fig. 3(d) in terms of λ .

Next, we present the behavior of magnetoresistivity. The relation of ρ_{xx} vs λ is shown in Fig. 4(a). Away from the VHS, its behavior is standard as in usual metals [38]: $\rho_{xx}\tau$ increases with λ^2 at $\lambda \ll 1$, saturates at $\lambda \gg 1$ with λ^{-2} , and grows approximately linearly in between. The B^2 behavior, i.e., the λ^2 dependence, in the weak field has been observed in LSCO [27,34]. Deviation from the B^2 behavior was found at $B \gtrsim 30$ T, corresponding to $\lambda \gtrsim 0.3$ in experiments [34]. However, when the system is close to the VHS, due to the divergence of m_c , the regime of linear growth is significantly enlarged, and the magnetoresistivity is greatly enhanced. The closeness to the VHS may provide an alternative explanation for the linear magnetoresistivity observed in the experiments at $0.16 < x < 0.19$ [34], rather than the more exotic picture of “Planckian dissipation,” i.e., $\tau^{-1} \propto B$ [35]. Within our scenario, we would expect the tendency of saturation of ρ_{xx} around $B \sim 100$ T (corresponding to $\lambda \approx 1$), which could be tested in the future. Figure 4(b) shows the doping dependence of $\rho_{xx}\tau$ at different values of λ . At $\lambda \ll 1$, $\rho_{xx}\tau$ smoothly depends on x since the average of the band mass plays the dominant role here. As λ increases, the cyclotron motion becomes more coherent. The enhancement of $|m_c|$ drives the divergence of $\rho_{xx}\tau$ as x approaches the VHS, which roughly follows $\frac{|m_c|}{1+x}$ for $x < x_{\text{VHS}}$ and $x > x_{\text{VHS}}$.

Since the cyclotron resonance has been observed in optimally doped LSCO [41], we argue that the role of cyclotron motion cannot be neglected in the study of the magnetotransport behavior. Certainly, in the strange metal region near optimal doping, our explanation based on the Fermi liquid picture may not directly apply. Nevertheless, our results could be further tested in the more heavily overdoped region and in higher fields.

IV. SUMMARY AND DISCUSSIONS

In summary, we have performed a semiclassical study of the Hall coefficient and magnetoresistivity near the VHS in overdoped LSCO based on the Fermi liquid assumption. Both R_H and $\rho_{xx}\tau$ strongly depend on the magnetic field: as B increases, R_H changes sign from positive to negative values at $x_{\text{VHS}} < x \lesssim 0.3$, and $\rho_{xx}\tau$ increases nearly linearly in the intermediate regime, especially near the VHS. Parts of the results are in good agreement with the known experiments and can be further checked to determine whether overdoped LSCO can be described by the Fermi liquid picture or not.

Before closing this paper, we provide some other remarks.

First, the band structure of LSCO is actually three-dimensional-like as we take into account the out-of-plane hopping t_z , whose value is on the same order as t'' , as shown by the ARPES measurement [39]. Although the effect of t_z smears out the VHS, the field dependence and sign change of R_H are not expected to change qualitatively.

Second, the VHS is not unique to LSCO but also appears in other hole-doped cuprates such as Nd-LSCO [15], $\text{Bi}_2\text{Sr}_2\text{CaCu}_2\text{O}_{8+\delta}$ (Bi2212) [45], $\text{Bi}_2(\text{Sr}, \text{La})_2\text{CuO}_{8+\delta}$ (Bi2201) [46,47], and YBCO [48,49]. Our study here indicates that the VHS needs more careful treatment when explaining their magnetotransport phenomena. Interestingly, Nd-LSCO and Bi2201 have a FS similar to (although with different t' and t'') LSCO, and thus, similar B and x dependences of R_H should be observed experimentally.

Third, although R_H obtained in the Fermi liquid picture is in good agreement with the experiments at high temperatures, its low-temperature upturn is difficult to understand even in the highly overdoped region [22–24]. Moreover, taking the overdoped sample $x = 0.23$ at 50 K as an example, the optical conductivity gives $\tau^{-1} \sim 5$ meV [44], giving rise to the theoretical value of $\rho_{xx} \sim 5\mu\Omega\text{cm}$ at $B = 0$, much smaller than the experimental value $\sim 50\mu\Omega\text{cm}$ [27]. In fact, this situation is similar to what happens in the superfluid density at zero temperature [26]. The Fermi liquid picture severely underestimates ρ_{xx} and R_H at low temperatures and overestimates the superfluid density. This dilemma may be resolved by additionally taking the vertex corrections (not just the band renormalization) into account, which is left for a future study.

Fourth, we have assumed an isotropic scattering rate in the present work to study the effect of the VHS, in particular to solve the mismatch between weak- and strong-field limits. At temperature as high as 300 K, the isotropic scattering rate is anticipated to dominate, and our predicted result for R_H vs x in the weak-field limit is consistent with the known experiments [22–24], as shown in Fig. 3(a). As temperature decreases, the isotropic scattering rate drops, and the anisotropic scattering becomes more and more relevant [50], which is expected to lead to enhancement of R_H since the nodal quasiparticles (holelike) contribute more and more.

Finally, we emphasize again that our description is based on the Fermi liquid picture and cannot be applied to the pseudogap and strange metal phases, which need a new theoretical framework beyond the standard Fermi liquid framework.

Note added. Recently, we became aware of an interesting experiment on Nd-LSCO [50] which measured both uniform and angle-dependent scattering rates and also explained the linear magnetoresistivity by electron cyclotron motions.

ACKNOWLEDGMENTS

We thank Y.-M. Dai, S.-D. Chen, and Y.-Y. Wang for helpful discussions. This work is supported by the National

Natural Science Foundation of China (under Grants No. 11874205, No. 11729402, and No. 11574134) and the National Key Research and Development Program of China (under Grant No. 2016YFA0300401).

- [1] P. A. Lee, N. Nagaosa, and X.-G. Wen, *Rev. Mod. Phys.* **78**, 17 (2006).
- [2] S. Badoux, W. Tabis, F. Laliberté, G. Grissonnanche, B. Vignolle, D. Vignolles, J. Béard, D. A. Bonn, W. N. Hardy, R. Liang, N. Doiron-Leyraud, L. Taillefer, and C. Proust, *Nature (London)* **531**, 210 (2016).
- [3] C. Collignon, S. Badoux, S. A. A. Afshar, B. Michon, F. Laliberté, O. Cyr-Choinière, J.-S. Zhou, S. Licciardello, S. Wiedmann, N. Doiron-Leyraud, and L. Taillefer, *Phys. Rev. B* **95**, 224517 (2017).
- [4] J. L. Tallon and J. W. Loram, *Physica C (Amsterdam, Neth.)* **349**, 53 (2001).
- [5] B. Keimer, S. A. Kivelson, M. R. Norman, S. Uchida, and J. Zaanen, *Nature (London)* **518**, 179 (2015).
- [6] C. Proust and L. Taillefer, *Annu. Rev. Condens. Matter Phys.* **10**, 409 (2019).
- [7] A. Eberlein, W. Metzner, S. Sachdev, and H. Yamase, *Phys. Rev. Lett.* **117**, 187001 (2016).
- [8] J. G. Storey, *Europhys. Lett.* **113**, 27003 (2016).
- [9] A. V. Maharaj, I. Esterlis, Y. Zhang, B. J. Ramshaw, and S. A. Kivelson, *Phys. Rev. B* **96**, 045132 (2017).
- [10] S. Verret, O. Simard, M. Charlebois, D. Sénéchal, and A.-M. S. Tremblay, *Phys. Rev. B* **96**, 125139 (2017).
- [11] J. Mitscherling and W. Metzner, *Phys. Rev. B* **98**, 195126 (2018).
- [12] S. Sachdev, *Rep. Prog. Phys.* **82**, 014001 (2018).
- [13] S. Chatterjee, S. Sachdev, and A. Eberlein, *Phys. Rev. B* **96**, 075103 (2017).
- [14] P. M. Bonetti, J. Mitscherling, D. Vilardi, and W. Metzner, *Phys. Rev. B* **101**, 165142 (2020).
- [15] C. E. Matt *et al.*, *Phys. Rev. B* **92**, 134524 (2015).
- [16] N. Doiron-Leyraud, O. Cyr-Choinière, S. Badoux, A. Ataei, C. Collignon, A. Gourgout, S. Dufour-Beauséjour, F. F. Tafti, F. Laliberté, M.-E. Boulanger, M. Matusiak, D. Graf, M. Kim, J.-S. Zhou, N. Momono, T. Kurosawa, H. Takagi, and L. Taillefer, *Nat. Commun.* **8**, 2044 (2017).
- [17] I. M. Lifshitz, M. I. Azbel, and M. I. Kaganov, *Sov. Phys. JETP* **4**, 41 (1957).
- [18] A. A. Abrikosov, *Fundamentals of the Theory of Metals* (North-Holland, Amsterdam, Netherlands, 1988).
- [19] J. M. Luttinger, *Phys. Rev.* **119**, 1153 (1960).
- [20] N. P. Ong, *Phys. Rev. B* **43**, 193 (1991).
- [21] T. Yoshida, X. J. Zhou, K. Tanaka, W. L. Yang, Z. Hussain, Z.-X. Shen, A. Fujimori, S. Sahrakorpi, M. Lindroos, R. S. Markiewicz, A. Bansil, S. Komiyama, Y. Ando, H. Eisaki, T. Kakeshita, and S. Uchida, *Phys. Rev. B* **74**, 224510 (2006).
- [22] H. Y. Hwang, B. Batlogg, H. Takagi, H. L. Kao, J. Kwo, R. J. Cava, J. J. Krajewski, and W. F. Peck, *Phys. Rev. Lett.* **72**, 2636 (1994).
- [23] T. Nishikawa, J. Takeda, and M. Sato, *J. Phys. Soc. Jpn.* **63**, 1441 (1994).
- [24] I. Tsukada and S. Ono, *Phys. Rev. B* **74**, 134508 (2006).
- [25] P. M. C. Rourke, I. Mouzopoulou, X. Xu, C. Panagopoulos, Y. Wang, B. Vignolle, C. Proust, E. V. Kurganova, U. Zeitler, Y. Tanabe, T. Adachi, Y. Koike, and N. E. Hussey, *Nat. Phys.* **7**, 455 (2011).
- [26] I. Božović, X. He, J. Wu, and A. T. Bollinger, *Nature (London)* **536**, 309 (2016).
- [27] R. A. Cooper, Y. Wang, B. Vignolle, O. J. Lipscombe, S. M. Hayden, Y. Tanabe, T. Adachi, Y. Koike, M. Nohara, H. Takagi, C. Proust, and N. E. Hussey, *Science* **323**, 603 (2009).
- [28] G. S. Boebinger, Y. Ando, A. Passner, T. Kimura, M. Okuya, J. Shimoyama, K. Kishio, K. Tamasaku, N. Ichikawa, and S. Uchida, *Phys. Rev. Lett.* **77**, 5417 (1996).
- [29] S.-W. Cheong, G. Aeppli, T. E. Mason, H. Mook, S. M. Hayden, P. C. Canfield, Z. Fisk, K. N. Clausen, and J. L. Martinez, *Phys. Rev. Lett.* **67**, 1791 (1991).
- [30] J. Wu, A. T. Bollinger, X. He, and I. Božović, *Nature (London)* **547**, 432 (2017).
- [31] J.-J. Wen, H. Huang, S.-J. Lee, H. Jang, J. Knight, Y. S. Lee, M. Fujita, K. M. Suzuki, S. Asano, S. A. Kivelson, C.-C. Kao, and J.-S. Lee, *Nat. Commun.* **10**, 3269 (2019).
- [32] F. F. Balakirev, J. B. Betts, A. Migliori, I. Tsukada, Y. Ando, and G. S. Boebinger, *Phys. Rev. Lett.* **102**, 017004 (2009).
- [33] F. Laliberté, W. Tabis, S. Badoux, B. Vignolle, D. Destraz, N. Momono, T. Kurosawa, K. Yamada, H. Takagi, N. Doiron-Leyraud, C. Proust, and L. Taillefer, *arXiv:1606.04491*.
- [34] P. Giraldo-Gallo, J. A. Galvis, Z. Stegen, K. A. Modic, F. F. Balakirev, J. B. Betts, X. Lian, C. Moir, S. C. Riggs, J. Wu, A. T. Bollinger, X. He, I. Božović, B. J. Ramshaw, R. D. McDonald, G. S. Boebinger, and A. Shekhter, *Science* **361**, 479 (2018).
- [35] J. Zaanen, *SciPost Phys.* **6**, 061 (2019).
- [36] I. Božović, J. Wu, X. He, and A. Bollinger, *Physica C (Amsterdam, Neth.)* **558**, 30 (2019).
- [37] R. G. Chambers, *Proc. Phys. Soc. A* **65**, 458 (1952).
- [38] R. G. Chambers, *Electrons in Metals and Semiconductors* (Chapman and Hall, London, 1990).
- [39] M. Horio *et al.*, *Phys. Rev. Lett.* **121**, 077004 (2018).
- [40] S. E. Sebastian and C. Proust, *Annu. Rev. Condens. Matter Phys.* **6**, 411 (2015).
- [41] K. W. Post, A. Legros, D. G. Rickel, J. Singleton, R. D. McDonald, X. He, I. Božović, X. Xu, X. Shi, N. P. Armitage, and S. A. Crooker, *Phys. Rev. B* **103**, 134515 (2021).
- [42] J. M. Ziman, *Electrons and Phonons: The Theory of Transport Phenomena in Solids* (Clarendon, Oxford, 1960).
- [43] P. Voruganti, A. Golubentsev, and S. John, *Phys. Rev. B* **45**, 13945 (1992).
- [44] F. Mahmood, X. He, I. Božović, and N. P. Armitage, *Phys. Rev. Lett.* **122**, 027003 (2019).
- [45] A. Kaminski, S. Rosenkranz, H. M. Fretwell, M. R. Norman, M. Randeria, J. C. Campuzano, J.-M. Park, Z. Z. Li, and H. Raffy, *Phys. Rev. B* **73**, 174511 (2006).

- [46] T. Kondo, T. Takeuchi, T. Yokoya, S. Tsuda, S. Shin, and U. Mizutani, *J. Electron Spectrosc. Relat. Phenom.* **137–140**, 663 (2004).
- [47] Y. Ding *et al.*, *Chin. Phys. Lett.* **36**, 017402 (2019).
- [48] K. Gofron, J. C. Campuzano, A. A. Abrikosov, M. Lindroos, A. Bansil, H. Ding, D. Koelling, and B. Dabrowski, *Phys. Rev. Lett.* **73**, 3302 (1994).
- [49] M. A. Hossain, J. D. F. Mottershead, D. Fournier, A. Bostwick, J. L. McChesney, E. Rotenberg, R. Liang, W. N. Hardy, G. A. Sawatzky, I. S. Elfimov, D. A. Bonn, and A. Damascelli, *Nat. Phys.* **4**, 527 (2008).
- [50] G. Grissonnanche, Y. Fang, A. Legros, S. Verret, F. Laliberté, C. Collignon, J. Zhou, D. Graf, P. Goddard, L. Taillefer, and B. J. Ramshaw, [arXiv:2011.13054](https://arxiv.org/abs/2011.13054).